Biomass burning emission estimates inferred from satellite column measurements of HCHO: Sensitivity to co-emitted aerosol and injection height

Siegfried Gonzi,[1] Paul I. Palmer,[1] Michael P. Barkley,[2] Isabelle De Smedt,[3] and Michel Van Roozendael[3]

Received 21 April 2011; revised 3 June 2011; accepted 10 June 2011; published 26 July 2011.

[1] We infer monthly regional biomass burning emissions of formaldehyde (HCHO) during 2006 from space-borne column measurements of HCHO from the SCIAMACHY instrument over Canada, boreal Asia, South America, southern Africa, and Indonesia. We remove the influence of biogenic volatile organic compounds using an offline chemical mechanism. We quantify the sensitivity of our emission estimates to aerosol single scattering albedo, ω, indicative of fresh ($\omega = 0.8$) and aged ($\omega > 0.9$) aerosol, and the relative vertical distribution of the aerosol and HCHO, both which compromise the interpretation of space-based HCHO columns. For our control calculation we assume freshly-emitted gases and aerosols that are mainly confined to the boundary layer. Associated posterior emissions are generally lower than the prior emissions except over Canada and boreal Asia during northern hemisphere summer months. Accounting for faster vertical mixing results in posterior emissions 20%–100% higher than the corresponding control calculation, and consequently more consistent with the prior. Assuming an aged aerosol generally results in a 20% decrease in posterior emissions relative to prior values. Based on the range of posterior estimates from our sensitivity analyses, not accounting for uncertainties associated with the underlying gas-phase and heterogeneous chemistry, we estimate HCHO emission uncertainties are typically 20%–30% but can be up to 300% in extreme cases. **Citation:** Gonzi, S., P. I. Palmer, M. P. Barkley, I. De Smedt, and M. Van Roozendael (2011), Biomass burning emission estimates inferred from satellite column measurements of HCHO: Sensitivity to co-emitted aerosol and injection height, *Geophys. Res. Lett.*, *38*, L14807, doi:10.1029/2011GL047890.

1. Introduction

[2] Current understanding of the variability and magnitude of biomass burning emissions is largely due to 1) bottom-up estimates inferred from the combination of space-borne observations of land-surface properties [e.g., *Roberts et al.*, 2009; *Giglio et al.*, 2010; *van der Werf et al.*, 2006] and emission factors derived from laboratory and field measurements [e.g., *Andreae and Merlet*, 2001; *Yokelson et al.*, 2003]; and 2) top-down estimates inferred from observed variations of atmospheric trace gases, indicative of incomplete combustion, interpreted using a chemistry transport model and an inverse model [e.g., *Müller and Stavrakou*, 2005]. Both methods incur substantial uncertainties.

[3] We infer biomass burning emissions from satellite observations of formaldehyde column measurements using the GEOS-Chem global 3-D chemistry transport model. HCHO is produced from the oxidation of methane and non-methane volatile organic compounds (NMVOCs) and emitted directly from incomplete combustion. Photodissociation and oxidation of HCHO by the OH radical is the dominant atmospheric loss resulting in an atmospheric lifetime of <1 day. This short lifetime permits the observed HCHO column variations to be related to local surface emissions on a spatial scale comparable with global chemistry transport models. Recent work estimated NMVOC emissions using HCHO columns observed by the SCanning Imaging Absorption spectroMeter for Atmospheric CHartographY (SCIAMACHY) using an adjoint inverse model framework [*Stavrakou et al.*, 2009b], distinguishing between biogenic and pyrogenic sources using prescribed spatial and temporal correlations of prior emission errors. For 2006 they estimated global emissions of 72–76 Tg/yr, which are 5–16% lower than their prior Global Fire Emission Database inventory estimates [*van der Werf et al.*, 2006].

[4] We adapt a methodology that was originally developed to infer emissions of biogenic VOCs [e.g., *Palmer et al.*, 2003, 2006]. We identify the emitted trace gases that explain the observed short-term (<1 day) variability of HCHO over fires, and remove scenes for which biogenic NMVOCs contribute more than 20% to this variability. We also account for the sensitivity of our methodology to assumptions about 1) interference due to absorbing and scattering aerosol emitted by combustion processes, and 2) rapid vertical mixing due to surface heating, which we show below has implications for the interpretation of observed HCHO columns. These sensitivity calculations effectively provide uncertainty bounds on our emission estimates.

2. Data and Methods

2.1. Forward Model and HCHO Production

[5] Our forward model relates surface emissions of HCHO and co-emitted HCHO precursors to atmospheric column measurements of HCHO. We use the GEOS-Chem global 3-D chemistry transport model v8.02.01, driven by

[1]School of GeoSciences, University of Edinburgh, Edinburgh, UK.
[2]Earth Observation Science Group, Space Research Centre, Department of Physics and Astronomy, University of Leicester, Leicester, UK.
[3]Belgian Institute for Space Aeronomy, Brussels, Belgium.

0094-8276/11/2011GL047890

GEOS-5 meteorology, with a horizontal resolution of 2 × 2.5° described on 47 vertical levels that span the surface to 0.01 hPa. We use the standard description of O_3-NO_x-VOC chemistry [*Bey et al.*, 2001] with minor modifications outlined below.

[6] Our model includes 24 biomass burning tracers, based on the Global Fire Emission Database v2 [*van der Werf et al.*, 2006], of which 13 (see Table S1 in the auxiliary material) have previously been identified as being important for the production of HCHO [*Stavrakou et al.*, 2009a].[1] For acetic acid [*Millet et al.*, 2008] and methanol [*Jacob et al.*, 2005], which the standard model does not include, we follow the method described below but include their HCHO contributions as an enhancement to direct emissions. In general, we estimate prior biomass burning emissions E_i for each species i by multiplying emission factors derived from field measurements (molec/kg of dry matter burned) [*Andreae and Merlet*, 2001; M. O. Andreae, personal communication, 2006] for three coarse land-types: savanna, tropical forest, and extratropical forest. We use dry matter burned estimates from the GFEDv2 inventory [*van der Werf et al.*, 2006] that assumes a dry matter carbon fuel content of 45%. We determine the amount of HCHO produced from each emitted species using short-term (<1 day) HCHO yields Y_i from the Master Chemical Mechanism [*Saunders et al.*, 2003; *Stavrakou et al.*, 2009a]. We calculate total pyrogenic HCHO emissions E_{HCHO}, using $E_{\mathrm{HCHO}} = \sum_{\mathrm{HCHO}} E_i Y_i$, as a function of time and location. We find that ethene, propene, and acetaldehyde form HCHO very rapidly and contribute 40%, 14–30% and 7% of the indirect HCHO production, respectively, and will therefore contribute significantly to the HCHO column variability over fire affected regions (see Table S1). We also find that direct emissions represent 14% and 29% of total pyrogenic HCHO emissions over tropical and boreal ecosystems, respectively, which does not vary during the burning season. The fraction of direct HCHO emissions is higher than previously reported values [*Stavrakou et al.*, 2009a], which used emission factors derived from field measurements [*Andreae and Merlet*, 2001] that have recently been shown to have a negative bias against laboratory data [*Wooster et al.*, 2011].

[7] For the purpose of this paper we focus on five regions (Figure S1): Canada (105–125°W, 42–60°N); boreal Asia (73–130°E, 50–65°N); Indonesia (100–140°E, 20–5°SN); South Africa (0–40°E, 30–0°S); South America (34–80°W, 30°S–5°N). We sample the model at the time and location of cloud-free SCIAMACHY scenes. We consistently sample model aerosol optical depths at 400 nm, close to the UV region used to retrieve HCHO from SCIAMACHY.

2.2. SCIAMACHY HCHO Columns

[8] We use data from the SCIAMACHY instrument [*Bovensmann et al.*, 1999], which was launched in a sun-synchronous orbit in 2002 aboard the ESA Envisat platform with a local equatorial overpass time of 10:30. HCHO slant columns, fitted to observed spectra at wavelengths 328.5–346 nm using differential optical absorption spectroscopy [*De Smedt et al.*, 2008], have a horizontal spatial resolution of 60 × 30 km^2. Slant columns are typically in the range of 10–40 × 10^{15} (molec cm^{-2}), and have a mean fitting error between 12% at low latitudes (2.5 × 10^{15} molec cm^{-2}) and 40% (8 × 10^{15} molec cm^{-2}) at high latitudes. To remove noise introduced by known instrument artefacts we use a reference sector method [*Barkley et al.*, 2008] that compares daily mean model and observed HCHO columns over the remote Pacific (140–160°W) as a function of latitude, and removing the resulting residual from all SCIAMACHY measurements. We also remove data with a solar zenith angle >64°.

[9] Vertical HCHO columns are determined from the fitted slant columns using an air mass factor (AMF) formulation that accounts for Rayleigh and aerosol scattering using a radiative transfer model [*Palmer et al.*, 2001]. We use a global climatology for surface albedo at UV wavelengths [*Koelemeijer et al.*, 2003]. We calculate an AMF for clear and cloudy scene, with the final AMF a weighted product of the two values [*Martin et al.*, 2002]. For the cloudy AMF, we use cloud top and optical depths from the GEOS-5 meteorology fields. Scenes with cloud fraction, estimated using the oxygen A band [*Wang et al.*, 2008; *Koelemeijer et al.*, 2002], greater than 40% are removed from subsequent analyses. We acknowledge that some cloudy scenes may be misidentified as aerosols and vice versa. However, we find our results do not change significantly by using a stricter cloud fraction threshold of 30%.

[10] The AMF is a strong function of the scattering properties of pyrogenic aerosol. We use a single scattering albedo (ω) indicative of fresh aerosol (ω = 0.8; few hours since emission) and aged aerosol (ω = 0.95 and 0.93 for boreal and tropical regions, respectively; >1 day since emission) [*Reid et al.*, 2005]. This increase in ω with time largely reflects the reduction of the black carbon content of the aerosol. We acknowledge that these ω values are for 440 nm, but values for wavelengths more appropriate for SCIAMACHY HCHO columns are not currently available. The AMF is also sensitive to the distribution of aerosol relative to HCHO. We define four aerosol vertical distributions which may result from assumptions about rapid vertical mixing due to surface fires (Figure S2): SN0) control run, where aerosol and HCHO emitted in the GEOS-Chem model are left unchanged; SN1) aerosol is mainly injected into the free troposphere; SN2) aerosol is distributed mainly within the boundary layer where the HCHO concentrations peak; and SN3) aerosol is injected according to regional injection heights inferred from independent observations [*Gonzi and Palmer*, 2010].

2.3. Inferring Wildfire Emissions From HCHO Columns

[11] To infer biomass burning emissions that are consistent with observed SCIAMACHY HCHO columns we adopt an approach developed to infer biogenic VOC emissions [*Palmer et al.*, 2003]. For the biogenic VOC method, we removed the influence of biomass burning emissions using thermal signatures of surface fire and coincident measurements of NO_2 [*Barkley et al.*, 2008]. Here, the situation is reversed and we remove the biogenic signal.

[12] First, we calculate the AMF for each individual SCIAMACHY slant column retrieval and compute the corresponding HCHO vertical column. We perform this calculation for three values of ω, and for four prescribed vertical distributions of aerosol described above. Second, we minimize the influence of biogenic VOCs by selecting

[1] Auxiliary materials are available in the HTML. doi:10.1029/2011GL047890.

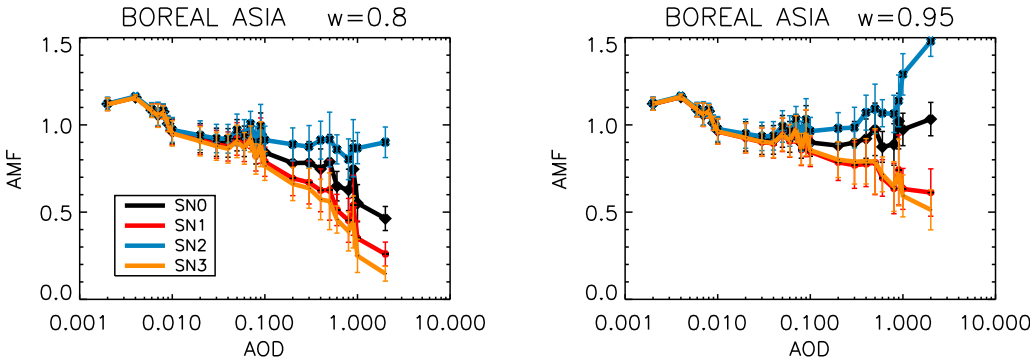

Figure 1. Sensitivity of the AMF to UV aerosol optical depth for the boreal region (Figure S1) in July 2006. (left) Results for fresh aerosol ($\omega = 0.8$), and (right) sensitivity for aged aerosol ($\omega = 0.95$). The black line describes the control run (SN0), the red line represents the simulation when aerosols are injected out of the boundary layer (SN1), the blue line describes the simulation of aerosol injected within the boundary layer (SN2), and the orange lines described the simulation where aerosol is injected according to *Gonzi and Palmer* [2010]. Error bars denote the 1σ standard deviation of the mean.

scenes where the fraction of HCHO emissions from pyrogenic VOCs is greater than 80% of the sum of HCHO emissions from biogenic and pyrogenic VOCs; we find our results do not change significantly if we consider alternate fractions of 70% and 90%. A second criterion is that we only consider SCIAMACHY scenes where there is collocated ATSR firecounts [*Schultz*, 2002]. Finally, we linearly regress model pyrogenic emissions (molec cm^{-2} sec^{-1}) and model HCHO columns (molec cm^{-2}) to obtain the slope and offset, which we transpose to infer pyrogenic emissions that are consistent with observed HCHO columns [*Palmer et al.*, 2003]. Monthly regional regression coefficients are shown in Table S2 and Figure S4 in the auxiliary material. We repeat this calculation for vertical columns that correspond to the two values of ω and the four aerosol vertical distributions.

3. Results

3.1. AMF Calculation

[13] Figure 1 shows the sensitivity of the AMFs, for example, over boreal Asia to aerosol optical depth (AOD), single scattering albedo (ω = 0.8 and 0.95), and aerosol vertical distribution; our general results do not change for the other four study regions (not shown). From this calculation, we draw four general conclusions. 1) Larger AODs result in smaller AMFs. A smaller AMF accounts for HCHO underlying aerosol extinction of incoming solar radiation. 2) Larger aerosol single scattering albedos result in larger AMFs. Scattering will allow some light through an aerosol layer, but multiple scattering may result in erroneous observational sensitivity [*Palmer et al.*, 2001]. 3) The AMF, as a function of injection height, becomes more sensitive to scattering properties when AODs >0.5. 4) Aerosols distributed below or coincident with peak HCHO concentrations increase observed sensitivity to HCHO, as expected.

3.2. Top-Down Emission Estimates

[14] Figure 2 shows box-and-whiskers plots of prior and posterior pyrogenic HCHO emissions (molec cm^{-2} sec^{-1}) from our study regions during 2006 corresponding to ω = 0.8. During regional burning seasons, prior bottom-up emissions are generally larger than the median posterior HCHO emissions. The exception is boreal Asia in May–September and Canada in June–July, respectively. We find that posterior HCHO emissions generally reproduce the seasonal cycle of the prior emissions.

[15] Posterior emissions are sensitive to both the assumed ω and vertical aerosol distribution. The relative aerosol/HCHO vertical distributions have the largest impact on posterior emissions, typically corresponding to the largest and smallest reported posterior values. In general we find that for each region, except Canada, during the burning season the top-down HCHO emissions that best match the bottom-up emissions correspond to the simulation accounting for vertical aerosol distribution, SN3 [*Gonzi and Palmer*, 2010], reflecting smaller associated AMFs (Figure 1). This effect is most noticeable over boreal Asia (May–July), Indonesia (October), South Africa (June–August), and South America (August–September) of 2006 (Figure 2). Generally, assuming a larger single scattering albedo, more representative of aged aerosol, results in HCHO emission estimates that are typically 10–20% lower than prior estimates (Figure S5) but can be much lower (e.g., Indonesia).

[16] Generally, the range of top-down emissions from our sensitivity calculations are either all above or all below prior emission estimates, providing clear guidance about how to scale the prior, but in some circumstances the difference between the lowest and highest observed HCHO emissions in a month can be as large as the corresponding bottom-up emission. For example, over boreal Asia during July observed HCHO emissions range from 16 to 50 $\times$ 10^{10} (molec cm^{-2} sec^{-1}), and the corresponding prior emission is 37 $\times$ 10^{10} (molec cm^{-2} sec^{-1}), so that depending on the assumption we make about ω and vertical mixing top-down emissions can be higher or lower than prior emissions. Typically, top-down emission uncertainties, which we base on the range of estimates from our sensitivity analyses, are 20–30% but can reach 300% for Indonesia during October. These uncertainty estimates do not include uncertainty in the gas and heterogeneous chemistry so must be considered as best-case values.

4. Concluding Remarks

[17] We have shown HCHO columns provide additional constraints on estimating biomass burning emissions. We

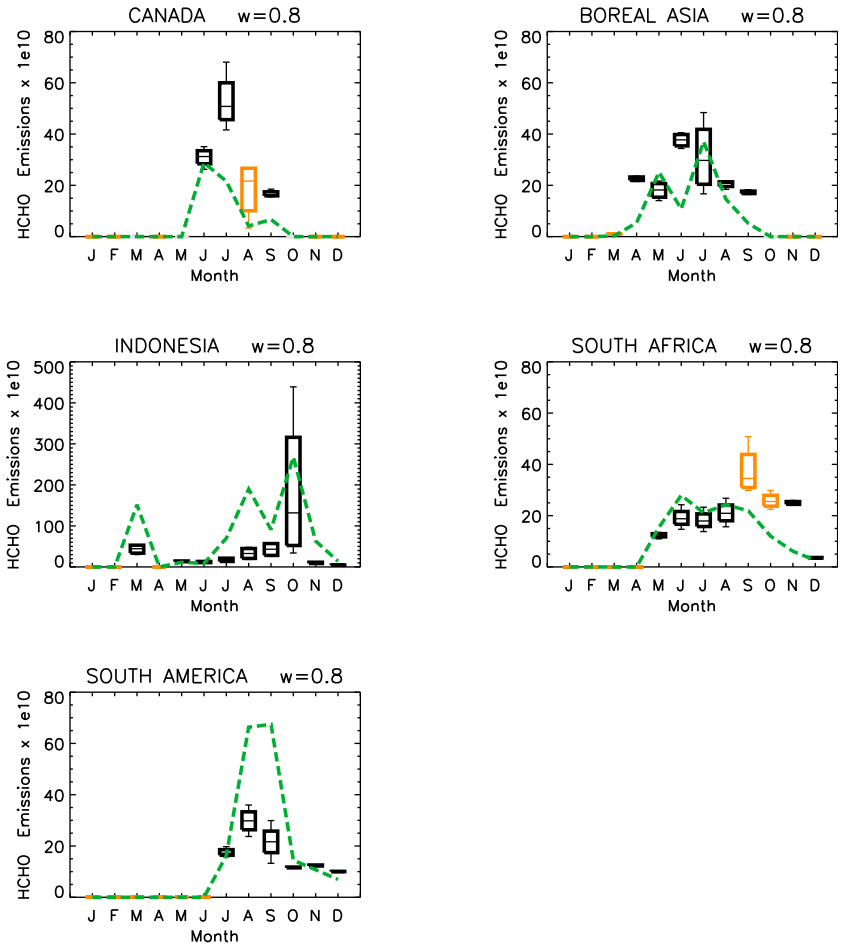

Figure 2. Monthly top-down estimates of HCHO emission (molec cm^{-2} sec^{-1}) over our five study regions, and their sensitivity to aerosol injection height (SN0, SN1, SN2, SN3) using $\omega = 0.8$. The box and whiskers plot, calculated using the injection scenarios, describes the minimum, first quartile, median, third quartile, and maximum emission estimate. The green dashed line describes the corresponding bottom-up estimates from the GFEDv2 model [*van der Werf et al.*, 2006]. Orange boxes denote top-down emission estimates where the regression parameters are statistically insignificant to the 90% level, determined using a two-tailed Student's t-test on the regression slope (Table S2).

argue these could be potentially more effective that CO. HCHO is rapidly produced near-field and has an atmospheric lifetime short enough that that observed variations can be related directly to surface emissions without having to consider model transport error, the latter being important for CO. We tested our approach over burning regions and compared our results against bottom-up prior emissions. To reconcile SCIAMACHY and bottom-up HCHO emission estimates we generally have to vertically inject aerosol out of the boundary layer and to use a single scattering albedo that is representative of freshly emitted aerosol. We find that in some instances top-down estimates resulting from our choice of aerosol single scattering albedo and vertical mixing can be very different and span the prior estimate.

[18] Quantifying pyrogenic emissions and their impact on atmospheric chemistry and radiation is a difficult problem to address using space-based measurements because they are generally a function of a number of parameters that 1) are not directly measured from space, e.g., fuel content, surface moisture, fire phase (flaming vs smouldering), and vertical mixing and its interaction with the mean flow on sub-model grid scales, and 2) compromise the interpretation of the observed scene, e.g., evolving mixing state and composition of pyrogenic aerosol. An integrative understanding of the interaction between the land-surface and atmospheric chemistry, radiation, and dynamics through dedicated fieldwork, laboratory, and modelling studies is clearly required to improve fundamental understanding of this problem.

[19] **Acknowledgments.** This work was supported by the UK Natural Environment Research Council (grant NE/E003990/1). We thank the anonymous reviewers, who provided thorough and thoughtful comments.

[20] The Editor thanks two anonymous reviewers for their assistance in evaluating this paper.

References

Andreae, M. O., and P. Merlet (2001), Emission of trace gases and aerosols from biomass burning, *Global Biogeochem. Cycles*, *15*, 955–966.

Barkley, M. P., P. I. Palmer, U. Kuhn, J. Kesselmeier, K. Chance, T. P. Kurosu, R. V. Martin, D. Helmig, and A. Guenther (2008), Net ecosystem fluxes of isoprene over tropical South America inferred from Global Ozone Monitoring Experiment (GOME) observations of HCHO columns, *J. Geophys. Res.*, *113*, D20304, doi:10.1029/2008JD009863.

Bey, I., D. Jacob, R. Yantosca, J. Logan, B. Field, A. Fiore, Q. Li, H. Liu, L. Mickley, and M. Schultz (2001), Global modeling of tropospheric

chemistry with assimilated meteorology: Model description and evaluation, *J. Geophys. Res.*, *106*, 23,073–23,095.
Bovensmann, H., et al. (1999), SCIAMACHY: Mission objectives and measurement modes, *J. Atmos. Sci*, *56*, 127–150.
De Smedt, I., et al. (2008), Twelve years of global observations of formaldehyde in the troposphere using GOME and SCIAMACHY sensors, *Atmos. Chem. Phys.*, *8*, 4947–4963.
Giglio, L., et al. (2010), Assessing variability and long-term trends in burned area by merging multiple satellite fire products, *Biogeosciences*, *7*, 1171–1186.
Gonzi, S., and P. I. Palmer (2010), Vertical transport of surface fire emissions observed from space, *J. Geophys. Res.*, *115*, D02306, doi:10.1029/2009JD012053.
Jacob, D. J., B. D. Field, Q. Li, D. R. Blake, J. de Gouw, C. Warneke, A. Hansel, A. Wisthaler, H. B. Singh, and A. Guenther (2005), Global budget of methanol: Constraints from atmospheric observations, *J. Geophys. Res.*, *110*, D08303, doi:10.1029/2004JD005172.
Koelemeijer, R. B. A., P. Stammes, J. W. Hovenier, and J. F. de Haan (2002), Global distributions of effective cloud fraction and cloud top pressure derived from oxygen A band spectra measured by the Global Ozone Monitoring Experiment: Comparison to ISCCP data, *J. Geophys. Res.*, *107*(D12), 4151, doi:10.1029/2001JD000840.
Koelemeijer, R. B. A., J. F. de Haan, and P. Stammes (2003), A database of spectral surface reflectivity in the range 335–772 nm derived from 5.5 years of GOME observations, *J. Geophys. Res.*, *108*(D2), 4070, doi:10.1029/2002JD002429.
Martin, R. V., et al. (2002), An improved retrieval of tropospheric nitrogen dioxide from GOME, *J. Geophys. Res.*, *107*(D20), 4437, doi:10.1029/2001JD001027.
Millet, D. B., et al. (2008), New constraints on terrestrial and oceanic sources of atmospheric methanol, *Atmos. Chem. Phys.*, *8*, 6887–6905.
Müller, J.-F., and T. Stavrakou (2005), Inversion of CO and NO_x emissions using the adjoint of the IMAGES model, *Atmos. Chem. Phys.*, *5*, 1157–1186.
Palmer, P. I., D. J. Jacob, K. Chance, R. V. Martin, R. J. D. Spurr, T. P. Kurosu, I. Bey, R. Yantosca, A. Fiore, and Q. Li (2001), Air mass factor formulation for spectroscopic measurements from satellites: Application to formaldehyde retrievals from the Global Ozone Monitoring Experiment, *J. Geophys. Res.*, *106*, 14,539–14,550, doi:10.1029/2000JD900772.
Palmer, P. I., D. J. Jacob, A. M. Fiore, R. V. Martin, K. Chance, and T. P. Kurosu (2003), Mapping isoprene emissions over North America using formaldehyde column observations from space, *J. Geophys. Res.*, *108*(D6), 4180, doi:10.1029/2002JD002153.
Palmer, P. I., et al. (2006), Quantifying the seasonal and interannual variability of North American isoprene emissions using satellite observations of the formaldehyde column, *J. Geophys. Res.*, *111*, D12315, doi:10.1029/2005JD006689.
Reid, J. S., et al. (2005), A review of biomass burning emissions part II: Intensive physical properties of biomass burning particles, *Atmos. Chem. Phys.*, *5*, 799–825.
Roberts, G., et al. (2009), Annual and diurnal African biomass burning temporal dynamics, *Biogeosciences*, *6*, 849–866, doi:10.5194/bg-6-849-2009.
Saunders, S. M., et al. (2003), Protocol for the development of the Master Chemical Mechanism, MCM v3 (part A): Tropospheric degradation of non-aromatic volatile organic compounds, *Atmos. Chem. Phys.*, *3*, 161–180, doi:10.5194/acp-3-161-2003.
Schultz, M. G. (2002), On the use of ATSR fire count data to estimate the seasonal and interannual variability of vegetation fire emissions, *Atmos. Chem. Phys. Discuss.*, *2*, 1159–1179.
Stavrakou, T., et al. (2009a), Evaluating the performance of pyrogenic and biogenic emission inventories against one decade of space-based formaldehyde columns, *Atmos. Chem. Phys.*, *9*, 1037–1060.
Stavrakou, T., et al. (2009b), Global emissions of non-methane hydrocarbons deduced from SCIAMACHY formaldehyde columns through 2003–2006, *Atmos. Chem. Phys.*, *9*, 3663–3679, doi:10.5194/acp-9-3663-2009.
van der Werf, G. R., et al. (2006), Interannual variability in global biomass burning emissions from 1997 to 2006, *Atmos. Chem. Phys.*, *6*, 3423–3441.
Wang, P., et al. (2008), FRESCO+: An improved O_2 A-band cloud retrieval algorithm for tropospheric trace gas retrievals, *Atmos. Chem. Phys.*, *8*, 6565–6576.
Wooster, M. J., et al. (2011), Field determination of biomass burning emission ratios and factors via open-path FTIR spectroscopy and fire radiative power assessment: Headfire, backfire and residual smouldering combustion in African savannahs, *Atmos. Chem. Phys. Discuss.*, *11*, 3259–3578, doi:10.5194/acpd-11-3529-2011
Yokelson, R. J., I. T. Bertschi, T. J. Christian, P. V. Hobbs, D. E. Ward, and W. M. Hao (2003), Trace gas measurements in nascent, aged, and cloud-processed smoke from African savanna fires by airborne Fourier transform infrared spectroscopy (AFTIR), *J. Geophys. Res.*, *108*(D13), 8478, doi:10.1029/2002JD002322.

M. P. Barkley, Earth Observation Science Group, Space Research Centre, Department of Physics and Astronomy, University of Leicester, Leicester LE1 7RH, UK.
I. De Smedt and M. Van Roozendael, Belgian Institute for Space Aeronomy, Avenue Circulaire, B-1180 Brussels, Belgium.
S. Gonzi and P. I. Palmer, School of GeoSciences, University of Edinburgh, West Mains Road, Edinburgh EH9 3JN, UK. (sgonzi@staffmail.ed.ac.uk)